ACS APPLIED MATERIALS & INTERFACES

Research Article

www.acsami.org

Vanadium Nitride Nanowire Supported SnS_2 Nanosheets with High Reversible Capacity as Anode Material for Lithium Ion Batteries

Muhammad-Sadeeq Balogun, Weitao Qiu, Junhua Jian, Yongchao Huang, Yang Luo, Hao Yang, Chaolun Liang, Xihong Lu,* and Yexiang Tong*

KLGHEI of Environment and Energy Chemistry, MOE of the Key Laboratory of Bioinorganic and Synthetic Chemistry, School of Chemistry and Chemical Engineering, Sun Yat-Sen University, Guangzhou 510275, People's Republic of China

Supporting Information

ABSTRACT: The vulnerable restacking problem of tin disulfide (SnS_2) usually leads to poor initial reversible capacity and poor cyclic stability, which hinders its practical application as lithium ion battery anode (LIB). In this work, we demonstrated an effective strategy to improve the first reversible capacity and lithium storage properties of SnS_2 by growing SnS_2 nanosheets on porous flexible vanadium nitride (VN) substrates. When evaluating lithium-storage properties, the three-dimensional (3D) porous VN coated SnS_2 nanosheets (denoted as CC-VN@SnS_2) yield a high reversible capacity of 75% with high specific capacity of about 819 mAh g^{-1} at a current density of 0.65 A g^{-1}. Remarkable cyclic stability capacity of 791 mAh g^{-1} after 100 cycles with excellent capacity retention of 97% was also achieved. Furthermore, discharge capacity as high as 349 mAh g^{-1} is still retained after 70 cycles even at a elevated current density of 13 A g^{-1}. The excellent performance was due to the conductive flexible VN substrate support, which provides short Li-ion and electron pathways, accommodates large volume variation, contributes to the capacity, and provides mechanical stability, which allows the electrode to maintain its structural stability.

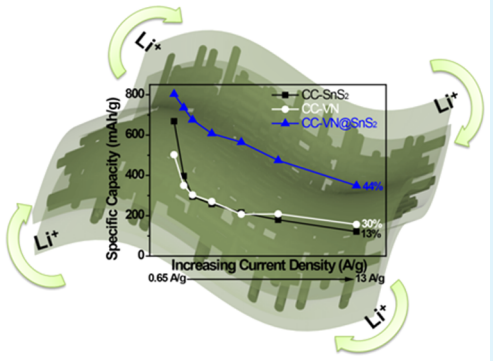

KEYWORDS: *tin disulfide, vanadium nitride, reversible capacity, anode, lithium ion batteries*

1. INTRODUCTION

Metal sulfides have recently emerged as promising anode material due to their excellent lithium redox reversibility and relatively high capacity.[1−6] SnS_2, as one of the prominent metal sulfide used as lithium ion battery anode,[7−10] has a layered CdI_2-type structure that consists of atomic layers of S−Sn−S stacked together by van der Waals interactions,[11] which allows Li ions to be reversibly intercalated into the galleries between the layers.[12] Recent investigation has revealed that SnS_2 nanostructures showed remarkably enhanced electrochemical properties as an electrode material in lithium ion batteries compared to their bulk counterparts, which is mainly due to their unique morphology, consisting of a finite lateral sized and well-defined layered structure.[13−15] However, its practical application is hampered primarily by the conversion reaction with structural reconstruction, restacking problem during cycling, which leads to poor initial reversibility and fast capacity fading.[10,11] Thus, it is necessary to improve the initial reversibility, and fast capacity fading of SnS_2 as lithium ion battery anode.

One of the prominent strategies to circumvent the problem is to synthesize various SnS_2 nanostructures.[16−18] For instance, SnS_2 nanoplates achieved a high initial reversible capacity of 645 mAh g^{-1} at a current density of 0.32 A g^{-1} with 85% capacity retention after 30 cycles.[10] Also, SnS_2 microspheres delivered an initial reversible capacity of 587 mAh g^{-1} at 0.65 A g^{-1} (28% Coulombic efficiency in the first cycle) and retained a capacity of 0.57 A g^{-1} after 100 cycles.[17] Another promising approach is to combine SnS_2 with highly conductive carbon materials such as carbon nanotubes and graphene[11,19−22] or other stable oxides.[23−25] For example, first reversible capacity of 650 mAh g^{-1} at current density of 0.05 A g^{-1} was delivered by 2D graphene−SnS_2 hybrid with Coulombic efficiency of about 37% and excellent rate capability up to 230 mAh g^{-1} at 6.4 A g^{-1}.[11] Meanwhile, SnS_2@MWCNTs nanocables also retains a reversible capacity of about 600 mAh g^{-1} at 0.1 A g^{-1} (37% Coulombic efficiency), which recorded 470 mAh g^{-1} capacity when the current rate was increased to 0.5 A g^{-1}.[26] Recently, SnS_2/GNS electrode achieved an initial reversible capacity up to 84% but at low current density.[12] With these progresses, the poor first/initial reversible capacity and low initial Coulombic efficiency of the SnS_2-based electrodes at high current densities are still unsatisfactory.[16,26−28] Also, the cyclic performance and rate capability of the most developed SnS_2-based electrodes still required further developments. It is still of great interest to develop an effective approach to increase the reversible capacity and lithium storage performance of the SnS_2.

Received: August 3, 2015
Accepted: October 6, 2015
Published: October 6, 2015

DOI: 10.1021/acsami.5b07044
ACS Appl. Mater. Interfaces 2015, 7, 23205−23215

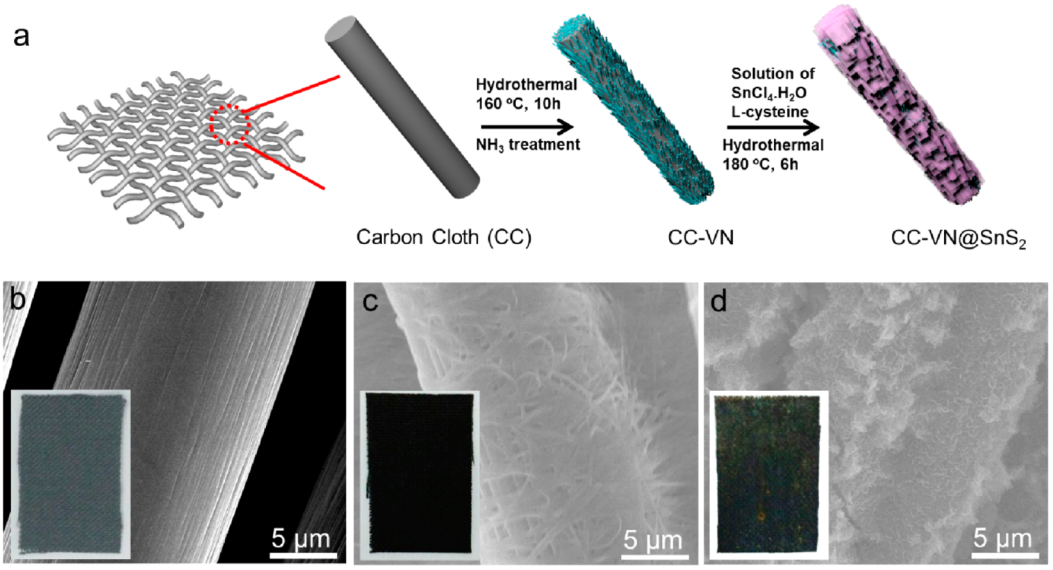

Figure 1. (a) Schematic diagram illustrates the two-step growth process for synthesizing the VN@SnS_2 NCs on carbon cloth substrate. SEM images of (b) the bare carbon cloth, (c) VN NWs on the carbon cloth, and (d) VN@SnS_2 on the carbon cloth. (Insets) Pictures of the corresponding carbon cloth that coated the materials.

Three-dimensional (3D) nanocomposites have many merits in improving electrochemical properties of high-performance electrodes[29] due to their substantial advantages that ensure much higher lithium ion flux across the electrode due to the dramatically increased electrode−electrolyte interface and also serve as the pathway for efficient electron transport, which could enhanced the diffusion kinetics for lithium storage.[30−34] To date, few works on 3D SnS_2-based electrode have been explored.[17,35,36] Hence, the fabrication of more 3D SnS_2-based nanostructures attracts some attention. In the present work, we report an effective approach to boost the poor reversible capacity of SnS_2 and improve its lithium storage performance of SnS_2, by providing VN nanowire substrates for the decoration of the SnS_2 nanosheet. To date, there is no literature on using metal nitride substrate as means of improving SnS_2-based electrodes. Metal nitrides grown on flexible carbon cloth substrate have been reported to be promising electrode materials with excellent electrical conductivity for energy storage devices,[37−39] while the effect of such substrates on electrochemical performance of metal sulfides has not yet been reported. We proposed that this interlaced VN nanowire substrate could not only protect the SnS_2 from morphological deformation, but also serve as active conductive material that could improve the lithium storage performance of the SnS_2. Hence, our as-fabricated porous VN decorated SnS_2 nanocomposite grown on the carbon cloth (denoted as CC-VN@SnS_2) delivers a high reversible capacity of 810 mAh g^{-1} with 71% Coulombic efficiency at a current density of 0.65 A g^{-1}, which is higher than the bare SnS_2 nanosheet, (denoted as CC-SnS_2) and VN nanowires (denoted as CC-VN). After 100 cycles, 97% capacity retention of its initial reversible capacity was achieved. More importantly, the discharge capacity of CC-VN@SnS_2 after 100 cycles is 791 mAh g^{-1}, which is 1.33 fold the summation capacity of the bare CC-SnS_2 (270 mAh g^{-1}) and CC-VN (323 mAh g^{-1}). Interestingly, the CC-VN@SnS_2 anode also exhibits excellent rate capability, which could deliver a high capacity of 349 mAh g^{-1} at a current density of 13 A g^{-1}.

2. EXPERIMENTAL SECTION

2.1. Synthesis of Porous VN Nanowires. Vanadium oxide (VO_x) NWs were synthesized by a hydrothermal method reported elsewhere with slight modification.[37] 0.324g NH_4VO_3 was dissolved in a 40 mL solution mixture of water and ethanol (volume ratio: 9/1). The solution pH was adjusted to ∼2 by HCl, and then transferred to a 30 ml Teflon-lined autoclave. A piece of clean carbon cloth was immersed into the precursor solution in the autoclave. The autoclave was heated at 160 °C for 3 h, and then let it cool down at room temperature. The carbon cloth was washed with deionized (DI) water and blow-dried with compressed air. A green VO_x NW film was uniformly coated on the carbon cloth. Porous VN NWs were obtained by annealing the as-prepared VO_x in NH_3 at 600 °C for 1 h. The color of the carbon cloth changes to black.

2.2. Synthesis of 3D Porous VN@SnS_2 Nanocomposite. The SnS_2 nanosheets were decorated on the VN nanowires according to the SnS_2 nanosheets preparation, except that the as-fabricated porous VN nanowires grown on the flexible carbon cloth was used as substrate. After hydrothermal process, a greenish-black SnS_2 film was collected washed with DI water and dried for subsequent experiments. The obtained material is denoted as porous CC-VN@SnS_2 nanocomposite.

2.3. Synthesis of SnS_2 Nanosheets. Tin chloride pentahydrate ($SnCl_4{\cdot}5H_2O$, 0.14 g) and L-cysteine (0.77 g) were dissolved in DI water (40 mL). A piece of clean carbon cloth was immersed into the precursor solution, transferred into a Teflon-lined stainless steel autoclave (50 mL), and hydrothermally treated in an electric oven at 160 °C for 6 h. A green SnS_2 film was collected, washed with DI water, and dried for subsequent experiments. The obtained product is tagged CC-SnS_2 nanosheets.

2.4. Material Characterization and Electrochemical Measurement. The morphology, structure, and composition of electrode materials were characterized by field-emission SEM (FE-SEM, JSM-6330F), TEM (TEM, JEM2010-HR, 200 kV), XPS (XPS, ESCALab250, Thermo VG) and Raman spectrometer (FT-IR, Nicolet 330). For electrochemical measurement, 2032 coin cell were used. The working electrodes were prepared by cutting the carbon cloth already covered uniformly with the samples into many smaller square pieces with area of 0.64 cm^2. Both the carbon cloth with loading samples and bare carbon cloth were weighed in a high-precision analytical balance (Sartorius, max weight 5100 mg, d = 0.001 mg). The mass loading of the grown material on the carbon cloth is around 3.1 mg cm^{-2}. The mass compositions of the SnS_2 and VN in the composite are SnS_2 2.0

DOI: 10.1021/acsami.5b07044
ACS Appl. Mater. Interfaces 2015, 7, 23205−23215

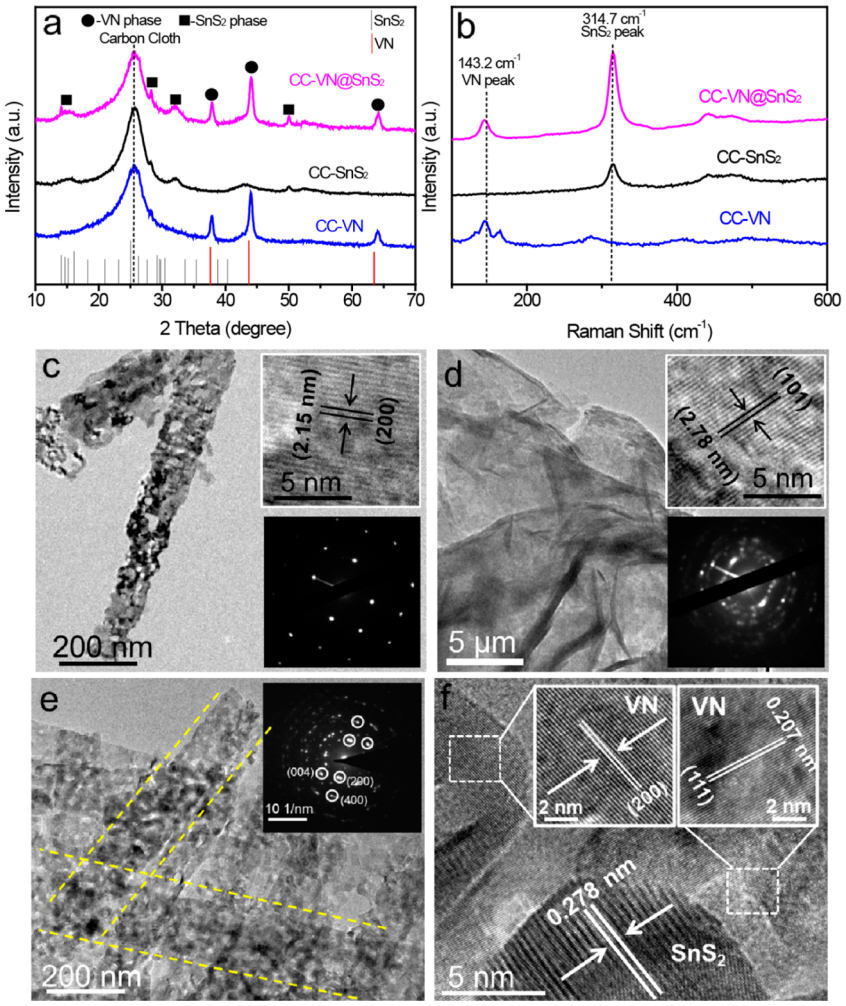

Figure 2. Characterization and morphology. (a) X-ray diffraction spectra and (b) Raman spectra of the CC-VN, CC-SnS_2, and VN@SnS_2 samples. (c) TEM image of the VN NW; (inset, top) HRTEM and (bottom) corresponding SAED pattern of the nanowire. (d) TEM image of the SnS_2 nanosheet; (inset, top) HRTEM and (bottom) corresponding SAED pattern of the nanosheet. (e) TEM image of the VN@SnS_2 and (inset) corresponding SAED pattern. (f) HRTEM image of the VN@SnS_2 and (insets) well-resolved lattice spacings of the VN and SnS_2.

and 1.5 mg cm^{-2}, respectively. Coin cells were assembled in an argon-filled glovebox [Mikrouna (China) Co., Ltd.] with Celgard 2400 separator containing a liquid electrolyte [a solution of 1 M $LiPF_6$ in 1:1 v/v of ethylene carbonate (EC)/dimethyl carbonate (DMC)] between the working electrode and a lithium foil, which serve as the counter and reference electrodes. The electrochemical performance was tested at different current densities in a voltage range of 0.01−3 V on a Neware battery testing system. Multicyclic voltammogram measurements and electrochemical impedance spectroscopy were performed with an electrochemical workstation (CHI 760D).

3. RESULTS AND DISCUSSION

3.1. Fabrication, Morphology, and Characterization of the VN@SnS_2 Nanocomposite. VN@SnS_2 nanocomposite was fabricated on a carbon cloth through two-step hydrothermal process as depicted in Figure 1a. In the first step, VN nanowires (NWs) were grown on the carbon cloth through hydrothermal synthesis of VO_x (Figure S1) and postannealing in NH_3 gas at 600 °C for 1 h according to our previous work with slight modification (Experimental Section).[37] The picture and scanning electron microscopy (SEM) image of the pristine carbon cloth was displayed in Figure 1b and inset. After hydrothermal and annealing processes, the carbon cloth color was covered uniformly with black films of VN NWs (Figure 1c, inset). SEM revealed that the carbon cloth fibers were uniformly coated by interlaced VN nanowires with average diameters between 400 and 600 nm (Figure 1c).

In order to obtain the VN@SnS_2 nanocomposite, the as-synthesized VN NWs were put into a solution of $SnCl_4{\cdot}5H_2O$ and L-cysteine at 180 °C for 6 h. The carbon cloth color changes from black to greenish black (Figure 1d, inset). SEM image shows that SnS_2 nanosheet uniformly covered onto the VN NWs surface (Figure 1d and Figure S3). For comparison SnS_2 nanosheets were also prepared according to the preparation of the VN@SnS_2 without in the absence of VN nanowires. Green films of SnS_2 nanosheets uniformly covered the carbon cloth (Figure S2a, inset) and SEM image affirmed uniform coating of nanosheet on the carbon cloth (Figure S2). The growth mechanism of the VN have been reported by our previous paper while the VN@SnS_2 nanocomposite is proposed to involve the biomolecular-assisted synthetic methods utilizing the L-cysteine (L-cys, $HSCH_2CHNH_2COOH$) with its multifunctional groups (SH, NH_2, and COO),[5,40] to conjugate with Sn metallic ions during the hydrothermal reaction. Then a sheet structure formed accordingly on the VN nanowires.

XRD and Raman spectra were collected for characterization of the samples. XRD spectra of the CC-VN@SnS_2 reveals the

DOI: 10.1021/acsami.5b07044
ACS Appl. Mater. Interfaces 2015, 7, 23205−23215

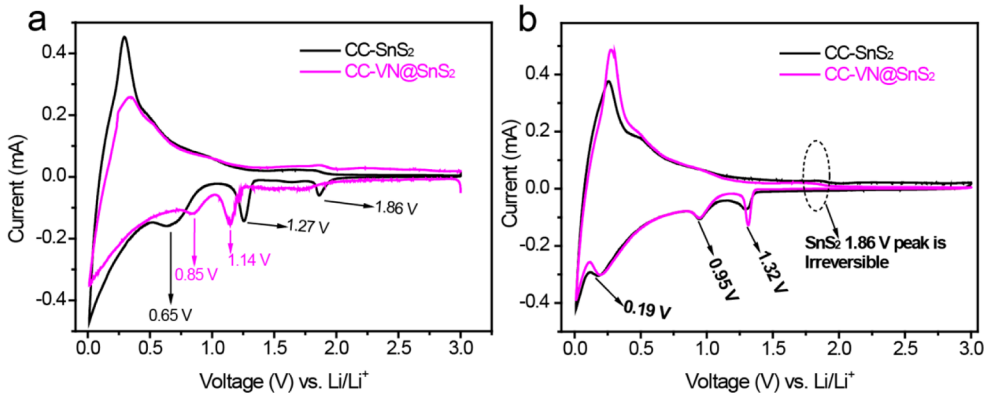

Figure 3. Lithium storage mechanism of the electrodes. (a) First and (b) second CV curves of the CC-SnS_2 and CC-VN@SnS_2 electrodes at a scan rate of 0.1 mV s^{-1} between 0.01 and 3.0 V.

diffraction peaks were basically peaks of VN (●) (JCPDS #35-0768), SnS_2 (■) and the carbon cloth (JCPDS #26-1076), while there are no traces of VN signal in the pristine SnS_2 spectra and vice versa for pristine VN spectra (Figure 2a). As shown in Figure 2b, Raman spectra collected for the VN@SnS_2 displays corresponding characteristic Raman peaks of the VN at 143 cm^{-1}[41] and SnS_2 at 314.7 cm^{-1}[16] were clearly recognized. Just as in the case of the XRD result, the Raman spectra of the VN exist without any traces of SnS_2 Raman signal and vice versa for SnS_2 Raman spectra. All these results confirm the successful fabrication of the nanocomposite. Transmission electron microscopy (TEM) and selected area electron diffraction (SAED) were carried out for further understanding about the structure and morphology of the samples. Figure 2c shows that the VN NWs are porous and single-crystalline in nature (Figure 2c, bottom inset) with lattice fringes of 2.15 nm corresponding to the (200) plane of the VN XRD spectra (JCPDS #35-0768; Figure 2c, top inset). Figure 2d also confirmed the nanosheet structure of the SnS_2 and their polycrystalline nature (Figure 2d, bottom inset) along with 2.78 nm lattice spacings that matches with the (101) plane of the SnS_2 XRD spectra (JCPDS #23-0677) (Figure 2d, top inset).

In Figure 2e, The porous VN NWs substrate coated with the SnS_2 can be seen clearly from the low-resolution TEM image, which also shows that the porous nature of the nanocomposite. SAED pattern confirm the polycrystalline nature of the nanocomposite and further affirms that the nanocomposite mainly consist of VN with (400) plane (JCPDS #35-0768) and SnS_2 with (004) and (200) planes (JCPDS #36-0677; Figure 2e, inset). High-resolution TEM (HRTEM) analysis recorded from Figure 2f displayed well-resolved lattice spacings of 0.235 and 0.207 nm, which correspond to the (101) and (200) plane of the cubic VN (JCPDS #65-0437), respectively; whereas the lattice fringes of the SnS_2 was 0.278 nm, which is in good agreement with the interplanar distance (101) planes of the hexagonal SnS_2 and our pristine SnS_2 nanosheets (JCPDS #23-0677) (Figure 2d). This further confirmed that the nanocomposite composed of VN and SnS_2 phases. Electron energy loss spectroscopy (EELS) elemental mapping collected for the nanowire edge at the circular dazed of Figure S4 show that the nanowire substrate are purely V and N, justifying the nanowire VN structure is still maintained after coating the SnS_2. These analyses confirm the successful formation of the VN@SnS_2 nanocomposite structure.

3.2. Lithium Storage Properties. We investigated the electrochemical properties of the CC-VN, CC-SnS_2, and CC-VN@SnS_2 samples as anode for lithium ion battery in half-cells, utilizing metallic lithium film as the counter electrode and reference electrode. To estimate the capacity contribution of the carbon cloth in the composite, the discharge−charge curves of the carbon cloth and the CC-VN@SnS_2 at the same current densities are also shown in Figure S5. The capacity contribution of the carbon cloth is ascribed to lithium insertion and extraction below 0.4 V,[42] with about 0.5 mA h capacity compare to that of CC-VN@SnS_2 with 4 mA h. Further calculation on the contribution of the carbon cloth is also displayed in the Supporting Information, which is also in accordance with other related work on carbon cloth.[43,44] One thing to point out is that the carbon cloth has a low capacity of ∼0.5 mA h, and its contribution was even less when it was covered with a thick layer of active materials.[42−44] Thus, in the following test, the capacity of the carbon cloth is less.

Cyclic voltammetry test was carried out to investigate the lithium storage mechanism and probably the reason(s) for the high reversible capacity of the CC-VN@SnS_2 electrode. Figure 3a shows the first cyclic voltammetry (CV) curves of the electrodes at a scanning rate of 0.1 mV/s. The storage mechanism of the individual SnS_2 and VN were discussed first. The storage mechanism between Li and SnS_2 include a conversion followed by an alloying/dealloying reaction (Figure 3a). The peak around 1.14 V can be attributed to the decomposition of SnS_2 into metallic Sn and Li_2S, while the peak below 1.0 V was related to the Li−Sn alloying.[45] The additional peaks at 1.86 V can be attributed to the lithium intercalation of the SnS_2 layers without phase decomposition. In the following cycles, the intercalation of Li ions from Sn occurred around 0.95 V. The electrochemical reaction of SnS_2 as anode can be described in the following equations;[19]

$$SnS_2 + 4Li^+ + 4e^- \rightarrow Sn + 2Li_2S \quad (1)$$

$$Sn + xLi^+ + xe^- \leftrightarrow LixSn\ (0 \le x \le 4.4) \quad (2)$$

For the backbone VN nanowire, Figure S6 shows the first through the third CV curves for the VN interlaced nanowires. There are two reduction peaks at 0.93 and 0.68 V in the initial discharging process. In subsequent cycles, the cathodic peaks at 0.68 V move to 0.95 V, while the one at 0.91 V disappears. This 0.95 V peak corresponds to Li extraction from and insertion into the nitride, which is very common for transition-metal−nitride (MN) electrodes as previously reported.[46] The reversible Li insertion/desertion process is usually written as follows:[47,48]

DOI: 10.1021/acsami.5b07044
ACS Appl. Mater. Interfaces 2015, 7, 23205−23215

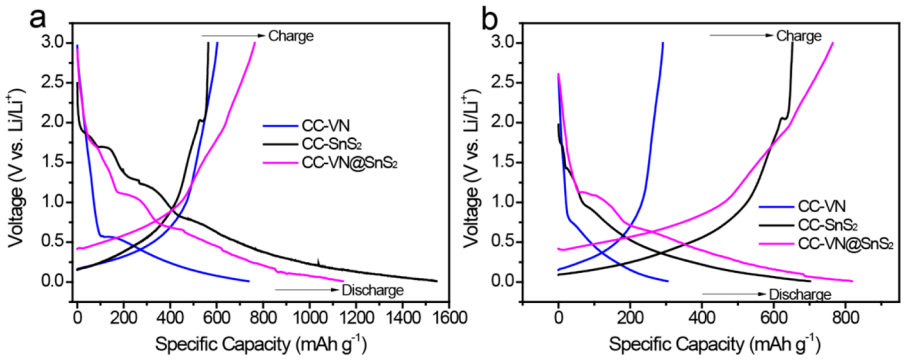

Figure 4. Discharge/charge profiles of the electrodes. (a) First and (b) Second discharge−charge voltage-capacity profiles of CC-VN, CC-SnS_2 and CC-VN@SnS_2 at a current density of 0.65 A g^{-1}.

$$VN + 3Li^+ + 3e^- \leftrightarrow V + Li_3N \quad (3)$$

For the CC-VN@SnS_2 nanocomposite, the cathodic peak at 1.27 V corresponds to the decomposition of SnS_2 into metallic Sn and Li_2S as well as the formation of solid electrolyte interface (SEI) layer,[10,12,49] which is the same as in the case of the CC-SnS_2, while the peaks below the potentials of around 0.7 V can be regarded as the signature of alloying (cathodic scan)/dealloying (anodic scan) of lithium from Sn metal.[50] As mentioned above, the CC-SnS_2 electrode showed an obvious cathodic peak at 1.86 V, while such a peak is nearly negligible in the CC-VN@SnS_2 electrode, which is also in good agreement with the charge−discharge voltage−capacity profiles (Figure 3a and 3b). This additional peak can be attributed to the lithium insertion of the SnS_2 layer without phase decomposition.[19,51] This peak was suggested also to be responsible for the higher capacity of the CC-SnS_2 electrode than that of the CC-VN@SnS_2. In the second cycle, the reduction peak at 1.86 V for the CC-SnS_2 electrode disappears in the second CV profile (Figure 3d), which was suggested to accounts for the low reversibility and Coulombic efficiency of the CC-SnS_2 electrode.[36] Moreover, the cathodic peaks at 0.65 and 1.27 V for the CC-SnS_2 electrode and 0.85 and 1.14 V for CC-VN@SnS_2 electrode shifts to 0.95 and 1.32 V, respectively. The voltage shift is a result of the continuous decomposition of SnS_2 into metallic Sn and Li_{2S} and the formation solid electrolyte interface (SEI) layer, which is common for metal sulfides.[10,49] The low voltage shift in CC-VN@SnS_2 electrode (i.e., from 0.85 to 0.95 V) is minimal, which suggest the reason for the low capacity loss in the CC-VN@SnS_2 electrode, while such shift is larger in the CC-SnS_2 electrode (from 0.65 to 0.95 V), leading to further loss of capacity of the CC-SnS_2 electrode in the second cycle and resulting in poor reversible capacity. Additionally, the CC-VN@SnS_2 electrode peak at 1.32 V is sharper than its counterpart electrode further suggesting the higher capacity observed in the CC-VN@SnS_2 electrode. This phenomenon is common to many lithium ion battery electrodes.[52] Furthermore, the synergetic effect of VN and SnS_2 can be related to the different cathodic reaction of VN and SnS_2 that synergistically gave rise to step-by-step storage processes. This increases the strain accommodation capability, structural stability, and cycling performance of the network during lithium insertion/extraction[25]

The first and second charge−discharge cycle profiles for the three electrodes at current density of 0.65 A g^{-1} are shown in Figure 4a,b. According to Figure 4a, the first discharge and charge capacities of the CC-VN@SnS_2 electrode were 1098 and 763 mAh g^{-1}, respectively, resulting in a Coulombic efficiency of 77%, while that of CC-SnS_2 is 35% and for CC-VN is 74%. During the second cycle, the CC-VN@SnS_2 electrode achieved a reversible capacity of 819 mAh g^{-1}, equivalent to 75% capacity reversibility, which is significantly higher than that of the CC-SnS_2 electrode (701 mAh g^{-1}) and CC-VN electrode (303 mAh g^{-1}) (Figure 4b). Unlike many reported SnS_2-based electrode that could only retain <40% reversible capacity after the first cycle, our reversible capacity reaches 75% (at a current density of 0.65 A g^{-1}), which is significantly higher than the recently reported SnS_2-based electrodes such as 2D graphene−SnS_2,[11] SnS_2−NS@MWCNTs,[19] SnS_2−SiO_2 nanorods,[53] SnS_2-graphene nanocomposites,[16,27] and comparable to the 3D SnS_2 hierarchitectures[26] and SnS_2/GNS electrode[54] that could only attained >75 and >84% at 0.1 A g^{-1} (see Table S1 in the Supporting Information for more comparison).[26,54] It is clearly shown in the charge/discharge profiles that the provision of the VN as substrate for the SnS_2 nanosheets effectively improved the reversible capacity CC-VN@SnS_2 electrode due to the excellent electrical conductivity of vanadium nitride (1.67×10^6 Ω^{-1} m^{-1})[37] and the synergistic effect of the both VN and SnS_2. It was also noted that the first discharge capacity of the CC-SnS_2 electrode was higher than that of CC-VN@SnS_2 counterpart. The reason for such higher capacity is not clear to us but we suggested that it might be due to the cathodic peak at about 1.86 V in the CC-SnS_2 discharge plateau (which is quite smaller in the CC-VN@SnS_2 voltage plateau) contributing to the high capacity of CC-SnS_2 in the first cycle. Another reason for higher initial capacity of CC-SnS_2 electrode compared with CC-VN@SnS_2 electrode should be related with the irreversible contribution from carbon cloth because of the lower coverage of carbon cloth of CC-SnS_2 electrode. It can also be concluded from the higher peak intensity of CC-SnS_2 from the CV curves in Figure 3c. Because the mass loading of the VN@SnS_2 is 3.1 mg cm^{-2}, that of VN is 48% and that of SnS_2 is 52%. Thus, we could calculate a theoretical capacity (C) of the VN@SnS_2 electrode as follows: $C_{Theoretical} = C_{VN} \times$ (% mass of VN) + $C_{SnS_2} \times$ (% mass of SnS_2) = $1238 \times 0.48 + 645 \times 0.52 = 931$ mAh g^{-1}. The theoretical capacity of the nanocomposite anode is 931 mAh g^{-1}, which is highly comparable to the experimental capacity 1098 mAh g^{-1}.

For high-performance electrode materials, cycling stability is one of the most important characteristics. Therefore, the cycling stability of the CC-VN, CC-SnS_2 electrode and CC-VN@SnS_2 electrodes was examined at a current density of 0.65 A g^{-1}. The CC-VN@SnS_2 electrode shows excellent cycling stability up to 100 cycles (Figure 5a). After 100 cycles, the

DOI: 10.1021/acsami.5b07044
ACS Appl. Mater. Interfaces 2015, 7, 23205−23215

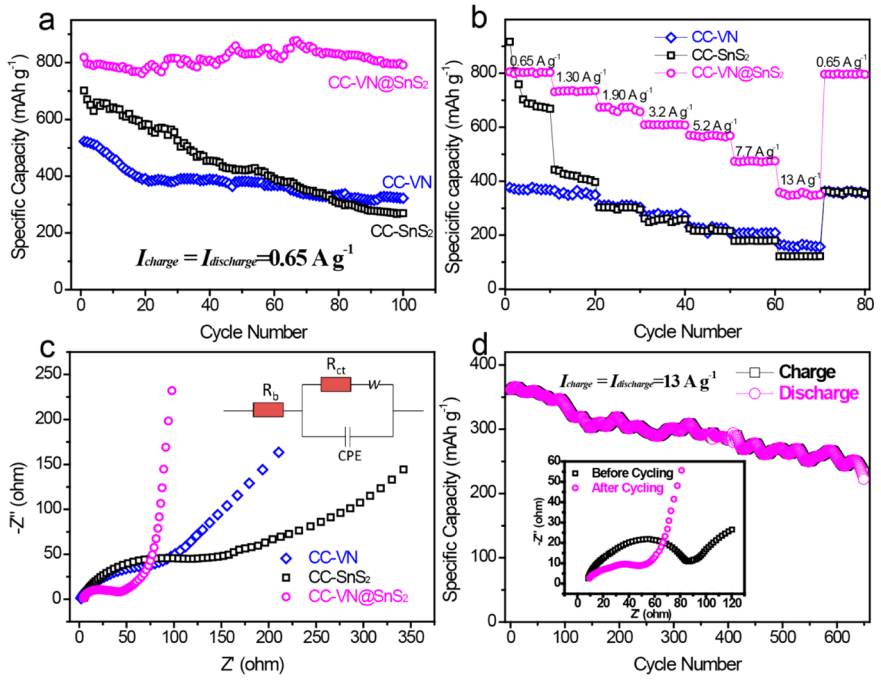

Figure 5. Electrochemical performance of the electrodes. (a) Cycling profiles up to 100 cycles at a current density of 0.65 A g^{-1}. (b) Rate capability profiles of the electrodes at different discharge and charge rates. (c) Nyquist plots of the electrodes and (inset) the equivalent circuit. (d) Cycling profiles of the CC-VN@SnS_2 electrodes up to 650 cycles at current density of 13 A g^{-1} and (inset) Nyquist plots of the CC-VN@SnS_2 electrode before and after cycling.

discharge capacities of the CC-SnS_2, CC-VN and CC-VN@SnS_2 electrodes are 270, 322, and 791 mAh g^{-1}, equivalent to 39, 67, and 97% capacity retention, respectively. Interestingly, the discharge capacity of the CC-VN@SnS_2 electrode is 1.33 fold higher than the addition of individual CC-SnS_2 and CC-VN electrode, which is even higher than the theoretical capacity of SnS_2 (645 mAh g^{-1}). Such capacity retention is higher than many previously reported SnS_2 nanostructures and their composites (see Table S1 for more comparison).[55−57] The XRD patterns of the two electrodes after charge/discharge process revealed that no changes were observed, and all the peaks in the pattern can be indexed to VN and SnS_2 (Figure S7). It should be mentioned that the peak at 20.5° come from the decomposition of the electrolyte ($LiPF_6$) embedded in the electrode in the air when doing XRD measurement. The XRD data confirmed no changes to metal oxide in the electrodes.

Rate capability is another very important consideration for practical lithium ion batteries. The CC-SnS_2 and CC-VN@SnS_2 electrodes were studied by charging/discharging at current density ranging from 0.65 to 13 A g^{-1}. As displayed in Figure 5b, the CC-VN@SnS_2 electrode exhibits continuous superior performance over the CC-SnS_2 and CC-VN electrodes. Moreover, the CC-VN@SnS_2 electrode exhibits a discharge capacity of 349 mAh g^{-1} even at a very high current density of 13 A g^{-1}, exhibiting about 44% retention of its initial capacity at 0.65 A g^{-1}, which is obviously higher than that of CC-SnS_2 electrode at 13%. At the same corresponding current densities, the retention value of CC-VN@SnS_2 electrode is also significantly higher than the values of recently reported SnS_2-based electrodes (see Table S1 for further comparison).[23,24,58,59]

It should be pointed out that such discharge capacity of the CC-VN@SnS_2 electrode (349 mAh g^{-1}) at such high current density (13 A g^{-1}) has never been reported for SnS_2-based anodes, and this work also constitute the one of the best report on SnS_2-based electrode at such high current density. It is worth noting that, apart from the discharge capacities at current density of 0.65 A g^{-1}, the discharge capacity of the CC-VN@SnS_2 electrode at such high rate of 13 A g^{-1} is 1 fold and above, higher than the sum of the CC-SnS_2 electrode (122 mAh g^{-1}) and CC-VN (157 mAh g^{-1}) at the same current density. Such excellent rate performance was suggested to be as a result of the excellent electrical conductivity of the porous VN NWs, which could serve as a flexible substrate for the SnS_2 nanosheets and prevent the electrode from structural damage when the current density increases.

To understand the reason for the enhanced rate capability of the CC-VN@SnS_2 electrode, resistance was analyzed by electrochemical impedance spectroscopy (EIS). The Nyquist plots of the three electrodes are shown in Figure 5c. The components of the equivalent circuit can be seen Figure 4c-inset. The charge transfer resistance (R_{ct}) values are calculated to be 210.4 Ω for the CC-SnS_2 electrode and 43.2 Ω for the CC-VN@SnS_2 electrode. It is apparent that the CC-VN@SnS_2 electrode has smaller R_{ct} than that of the pristine SnS_2 electrodes, indicating that the nanocomposite possesses higher electronic conductivity and may account for the excellent performance of the CC-VN@SnS_2 electrode. In addition, Warburg system dominates the impedance plot for a reversible electrochemical system. Increase in the slope of Warburg line indicates fast lithium ion diffusion.[60−62] Thus, compare to the CC-VN and CC-SnS_2 electrodes, in which their Warburg slope appears at about 45°, the Warburg line of the CC-VN@SnS_2 electrode displays a slope at an angle near 90°, suggesting the fast lithium ion diffusion in the nanocomposite.

To study the effect of high current rate cyclic performance of the nanocomposite, the CC-VN@SnS_2 electrode was charge−discharge for 650 cycles at a high current density of 13 A g^{-1}.

DOI: 10.1021/acsami.5b07044
ACS Appl. Mater. Interfaces 2015, 7, 23205−23215

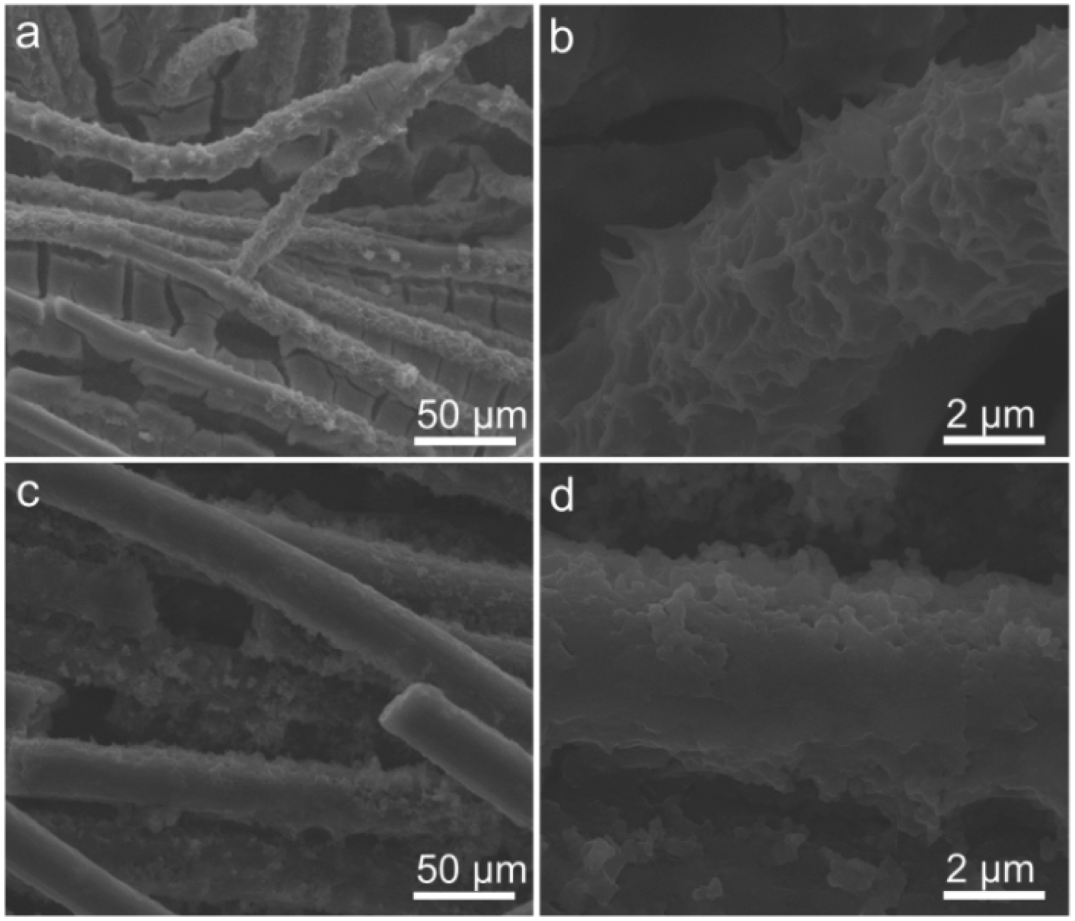

Figure 6. Morphology of the electrodes after electrochemical cycling; SEM images of the (a and b) CC-VN@SnS_2 and (c and d) CC-SnS_2 after 100 cycles at current density of 0.65 A g^{-1}.

First, the cyclic capacity profiles at current density 13 A g^{-1} rates up until 650 cycles are reasonably good, remaining at 231 mAh g^{-1} (about 64% capacity retention) from its initial capacity at 361 mAh g^{-1} (Figure 5d). This is one of the longest cycle life reported for SnS_2-based nanostructures but the cyclic stability capacity retention can be further improve in future research.

On the basis of this result, we believe that further investigation can still be carried out to improve the cyclic performance of SnS_2 at higher current densities. Figure 5d-inset shows the Nyquist plot of the CC-VN@SnS_2 electrode before and after cycling. Obviously, the impedance of the electrode decreases evidently after cycling. The reason for the decrease in the impedance could be due to the reduction of SnS_2 and VN into Sn and V by the irreversible reactions, respectively. SEM images of the CC-VN@SnS_2 and CC-SnS_2 electrode after considerable pulverization of the electrodes due to continuous lithiation/delithiation processes are shown in Figure 6 in order to study the structural stability effect on the performance of the electrodes. Figure 6a,b shows that the structure of the CC-VN@SnS_2 nanocomposite still adheres firmly to the surface of the carbon cloth, and the nanowire decorated nanosheets structure can still be well recognized, indicating the excellent stability of the CC-VN@SnS_2 electrode. Such structural stability of the CC-VN@SnS_2 electrode accounts for its high capacity retention over the CC-SnS_2 electrode. For the CC-SnS_2 electrode, the nanosheet structure of the SnS_2 cannot be identified (Figure 6c,d). This indicated that there is structural deformation of the SnS_2 electrode, which is suggested to be one of the main reasons for their poor lithium storage performance.

To obtain insight into the reasons for the improved lithium storage performance of the CC-VN@SnS_2 electrode, we performed X-ray photoelectron spectroscopy (XPS) measurements to study the effect of the porous VN on the composition and oxidation state of the nanocomposite. The XPS survey spectra of the samples are shown in Figure S8. Figure 7a shows the normalized V 2p core level XPS spectra of VN and VN@SnS_2 samples. Three peaks centered between ~513.99 and ~517.5 eV and between ~521.45 and ~ 525.05 eV were noticed for the two samples corresponding to the V $2p^3$ and V $2p^1$ peaks, respectively.[63,64] In comparison to the VN sample, the peaks of the VN@SnS_2 sample shifted to the lower binding energy with decrease in signal intensity. The shift to the lower binding energy peaks suggest the reduction of higher valence V^{5+}-type to lower stable oxidation states V^{4+}, V^{3+}, and V^{2+}.[63−67] The presence of these lower stable oxidation states in the V 2p spectra of the VN@SnS_2 sample suggests improve in the conductivity of the VN@SnS_2 sample,[67,68] which accounts for its high lithium storage performance over the SnS_2 and VN counterparts. Such a shift to the lower binding energy can also be observed in the V−N bond of the normalized N 1s XPS spectra of the CC-VN@SnS_2 sample (Figure 7b).[37,65]

Moreover, apart from the main component centered at 530.45 eV (OI) for the O 1s spectra, an additional peak at 531.72 eV (OII) was also observed for the VN and SnS_2, while that of VN@SnS_2 sample exists at 532.33 eV (Figure 7c).

DOI: 10.1021/acsami.5b07044
ACS Appl. Mater. Interfaces 2015, 7, 23205−23215

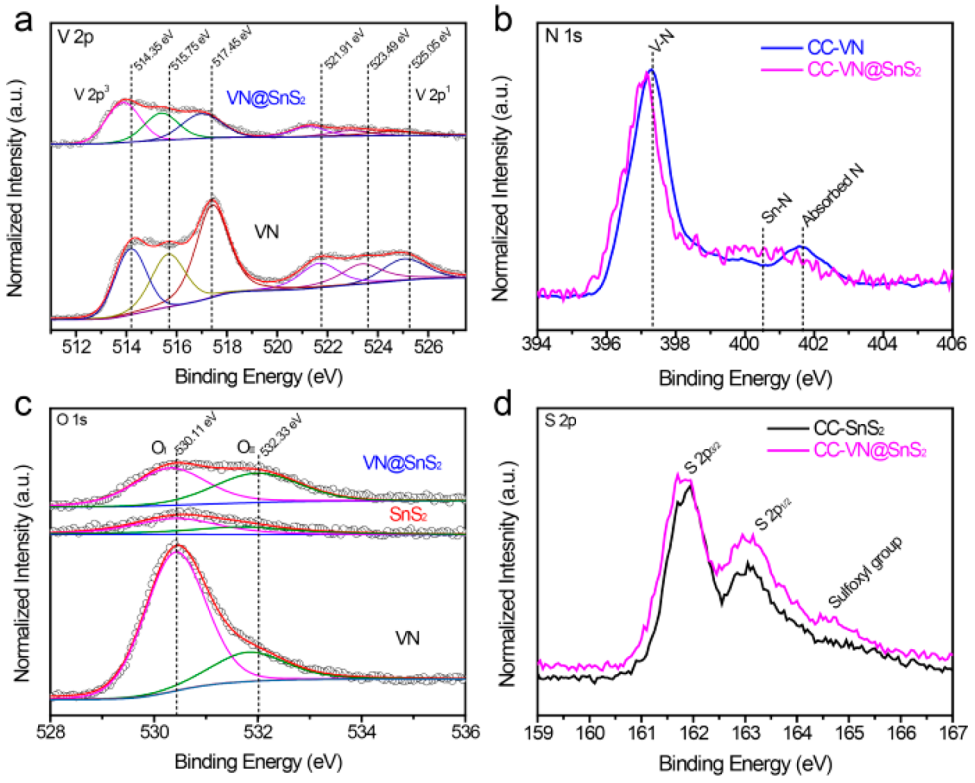

Figure 7. XPS characterization of the samples. (a) V 2p, and (b) N 1s XPS core-level spectra of VN and VN@SnS_2 samples. (c) O 1s core-level spectra of the three samples. (d) S 2p XPS Core-level spectra of SnS_2 and VN@SnS_2 samples.

Compared to the VN and SnS_2 samples, the OI signal intensity of the VN@SnS_2 sample reduces, while the OII increases, suggesting the increase in the −OH content on the VN@SnS_2 surface. Additionally, the normalized S 2p spectra of the VN@SnS_2 sample also confirmed the lower binding energy shift and increased broad signal intensity over the SnS_2 sample (Figure 7d). The peak difference indicates some modifications in the nanocomposite, which suggest some of the reason for the improved lithium storage properties. Furthermore, all these results further confirm that VN@SnS_2 sample is composed of active components, which are suggested to be the effective channel for improving the conductivity and fast diffusion of lithium ion in the VN@SnS_2.

Further improvement in the lithium storage performance for the CC-VN@SnS_2 nanocomposite could also be attributed to the following: (1) The porous 3D interconnected network, which possesses the merit of both nanosized back-up blocks and 2D assemblies toward lithium storage thereby enhances charge-transport capabilities upon cycling.[29] The formation rough 3D nanostructure, suggest higher surface area, which prevent the SnS_2 nanosheets from vulnerable restacking (unlike the smooth SnS_2 surface, which is easy to restacked, thereby reducing effective surface areas of the pristine SnS_2 to form any polymeric films). (2) The introduction of flexible electrically conductive porous VN nanowires substrate, which gives enough support for the SnS_2 nanosheets to provide a short Li^+ diffusion path, preventing their agglomeration and fast fading in capacity, thereby maintaining structural integrity during the electrochemical process and significantly improving the reversible capacity, Coulombic efficiency, and cyclic stability of the CC-VN@SnS_2 electrode.[69] The VN nanowire 1D nanostructures usually possess unique physical and chemical characteristics, which can restrict the formation of a solid electrolyte interphase (SEI) and volume expansion.[70,71] (3) The growth of the nanocomposite on the carbon cloth, which is well in contact with the active materials, provides mechanical support, avoiding the use of polymer binder/conductive additives and, hence, significantly reduces the inactive interface.[43,67] Furthermore, the individual and synergistic effect of the materials, which are someworth good active materials, resulting to high lithium storage performance of the CC-VN@SnS_2.[72]

4. CONCLUSIONS

In summary, we have demonstrated a new and effective strategy to improve the reversible capacity and lithium storage properties of SnS_2 by utilizing free-standing porous VN interlaced nanowire as substrate for the growth of SnS_2 nanosheets. VN nanowires were first obtained on the flexible carbon cloth, followed by another hydrothermal synthesis of SnS_2, to form the porous CC-VN@SnS_2 nanocomposite. This CC-VN@SnS_2 electrode exhibited excellent electrochemical performance over the bare CC-SnS_2 and CC-VN counterparts. A high initial reversible capacity of 819 mAh g^{-1}, with Coulombic efficiency of 72%, which could only lose 3% capacity after 100 cycles at a current density of 0.65 A g^{-1} was achieved by the porous CC-VN@SnS_2 nanocomposite. The nanocomposite also exhibits excellent rate performance, displaying a capacity of 349 mAh g^{-1} and attractive long cyclic performance at 13 A g^{-1}. This highly improved electrochemical performance of the nanocomposite is ascribed to the excellent electrical conductivity of the flexible porous VN NW substrate and the design of 3D structure, which allows the easy flow of Li ion in the SnS_2 layers. On the basis of this work, there is still a prominent challenge for further improvement on the cyclic performance of SnS_2-based at ultrahigh current densities. It should be mentioned that compared to other metal oxides or

DOI: 10.1021/acsami.5b07044
ACS Appl. Mater. Interfaces 2015, 7, 23205−23215

sulfides, the cyclic stability reported at high current density of 13 A g^{-1} still requires further improvement in terms of capacity retention. Also, using carbon cloth as current collector may lead to lower volumetric capacity. In such cases, a lighter weight conductive substrate can be utilized to replace the carbon cloth. The novel combinations of VN nanowires and SnS_2 nanosheets should also inspire the design and fabrication of the next generation of lithium ion battery anode based on metal nitride and metal sulfide nanocomposites.

■ ASSOCIATED CONTENT

Supporting Information

The Supporting Information is available free of charge on the ACS Publications website at DOI: 10.1021/acsami.5b07044.

SEM images of the VN, SnS_2 and VN@SnS_2 samples. EELS of the VN@SnS_2 samples, capacity contribution of the carbon cloth, CV curves of the VN, XRD patterns of the CC-SnS_2 and CC-VN@SnS_2 after charge−discharge process, XPS Survey spectra of the CC-SnS_2, CC-VN and CC-VN@SnS_2 samples and table comparing the electrochemical properties of SnS_2 nanostructure and its composites. (PDF)

■ AUTHOR INFORMATION

Corresponding Authors

*E-mail: luxh6@mail.sysu.edu.cn.
*E-mail: chedhx@mail.sysu.edu.cn. Phone: 86-20-84110071. Fax: 86-20-84112245.

Author Contributions

The experiments were designed by M.-S.B. with suggestions from Prof. Xihong Lu and Prof. Yexiang Tong. M.-S.B. and J.J. prepared the electrode materials and performed the lithium storage measurements. W.Q. performed the SEM analysis. C.L. and Y.L. carried out the transmission electron microscopy (TEM) study and analysis. Y.H. and H.Y. performed the XPS and Raman analyses. M.-S.B., X.L., and Y.T. analyzed the data and wrote the manuscript. All authors discussed the results and commented on the manuscript.

Notes

The authors declare no competing financial interest.

■ ACKNOWLEDGMENTS

We acknowledge the financial support of this work received by the Natural Science Foundation of China (21273290, 21403306, and J1103305) and the Natural Science Foundations of Guangdong Province (S2013030013474), Guangdong Natural Science Foundation for Distinguished Young Scholar (2014A030306048).

■ REFERENCES

(1) Stephenson, T.; Li, Z.; Olsen, B.; Mitlin, D. Lithium Ion Battery Applications of Molybdenum Disulfide (MoS_2) Nanocomposites. *Energy Environ. Sci.* **2014**, *7*, 209−231.

(2) Zhao, L.; Yu, X.; Yu, J.; Zhou, Y.; Ehrlich, S. N.; Hu, Y.-S.; Su, D.; Li, H.; Yang, X.-Q.; Chen, L. Remarkably Improved Electrode Performance of Bulk MnS by Forming a Solid Solution with FeS−Understanding the Li Storage Mechanism. *Adv. Funct. Mater.* **2014**, *24*, 5557−5566.

(3) Gao, M.-R.; Xu, Y.-F.; Jiang, J.; Yu, S.-H. Nanostructured Metal Chalcogenides: Synthesis, Modification, and Applications in Energy Conversion and Storage Devices. *Chem. Soc. Rev.* **2013**, *42*, 2986−3017.

(4) Zhang, L.; Wu, H. B.; Yan, Y.; Wang, X.; Lou, X. W. Hierarchical MoS_2 Microboxes Constructed by Nanosheets with Enhanced Electrochemical Properties for Lithium Storage and Water Splitting. *Energy Environ. Sci.* **2014**, *7*, 3302−3306.

(5) Qiu, W.; Xia, J.; Zhong, H.; He, S.; Lai, S.; Chen, L. L-Cysteine-assisted Synthesis of Cubic Pyrite/Nitrogen-Doped Graphene Composite as Anode Material for Lithium-ion Batteries. *Electrochim. Acta* **2014**, *137*, 197−205.

(6) Xiao, J.; Wang, X.; Yang, X.-Q.; Xun, S.; Liu, G.; Koech, P. K.; Liu, J.; Lemmon, J. P. Electrochemically Induced High Capacity Displacement Reaction of PEO/MoS_2/Graphene Nanocomposites with Lithium. *Adv. Funct. Mater.* **2011**, *21*, 2840−2846.

(7) Deng, W.; Chen, X.; Liu, Z.; Hu, A.; Tang, Q.; Li, Z.; Xiong, Y. Three-Dimensional Structure-Based Tin Disulfide/Vertically Aligned Carbon Nanotube Arrays Composites as High-Performance Anode Materials for Lithium Ion Batteries. *J. Power Sources* **2015**, *277*, 131−138.

(8) Zhao, Y.; Li, X.; Yan, B.; Li, D.; Lawes, S.; Sun, X. Significant Impact of 2D Graphene Nanosheets on Large Volume Change Tin-Based Anodes in Lithium-Ion Batteries: A Review. *J. Power Sources* **2015**, *274*, 869−884.

(9) Lefebvre, I.; Lannoo, M.; Moubtassim, M. E.; Fourcade, J. O.; Jumas, J. C. Lithium Insertion in Three-Dimensional Tin Sulfides. *Chem. Mater.* **1997**, *9*, 2805−2814.

(10) Seo, J.-w.; Jang, J.-t.; Park, S.-w.; Kim, C.; Park, B.; Cheon, J. Two-Dimensional SnS_2 Nanoplates with Extraordinary High Discharge Capacity for Lithium Ion Batteries. *Adv. Mater.* **2008**, *20*, 4269−4273.

(11) Luo, B.; Fang, Y.; Wang, B.; Zhou, J.; Song, H.; Zhi, L. Two Dimensional Graphene-SnS_2 Hybrids with Superior Rate Capability for Lithium Ion Storage. *Energy Environ. Sci.* **2012**, *5*, 5226−5230.

(12) Zhai, C.; Du, N.; Yang, H. Z. D. Large-Scale Synthesis of Ultrathin Hexagonal Tin Disulfide Nanosheets with Highly Reversible Lithium Storage. *Chem. Commun.* **2011**, *47*, 1270−1272.

(13) Huang, Y.; Ling, C.; Chen, X.; Zhou, D.; Wang, S. SnS_2 Nanotubes: a Promising Candidate for the Anode Material for Lithium Ion Batteries. *RSC Adv.* **2015**, *5*, 32505−32510.

(14) Zhu, W.; Yang, Y.; Ma, D.; Wang, H.; Zhang, Y.; Hu, H. Controlled Growth of Flower-like SnS_2 Hierarchical Structures with Superior Performance for Lithium-Ion Battery Applications. *Ionics* **2015**, *21*, 19−26.

(15) Huang, Z. X.; Wang, Y.; Wong, J. I.; Yang, H. Y. Free Standing SnS_2 Nanosheets on 3D Graphene Foam: an Outstanding Hybrid Nanostructure Anode for Li-Ion Batteries. *2D Mater.* **2015**, *2*, 024010.

(16) Du, Y.; Yin, Z.; Rui, X.; Zeng, Z.; Wu, X.-J.; Liu, J.; Zhu, Y.; Zhu, J.; Huang, X.; Yan, Q.; Zhang, H. A Facile, Relative Green, and Inexpensive Synthetic Approach Toward Large-Scale Production of SnS_2 Nanoplates for High-Performance Lithium-Ion Batteries. *Nanoscale* **2013**, *5*, 1456−1459.

(17) Zai, J.; Wang, K.; Su, Y.; Qian, X.; Chen, J. High Stability and Superior Rate Capability of Three-Dimensional Hierarchical SnS_2 Microspheres as Anode Material in Lithium Ion Batteries. *J. Power Sources* **2011**, *196*, 3650−3654.

(18) Zai, J.; Qian, X.; Wang, K.; Yu, C.; Tao, L.; Xiao, Y.; Chen, J. 3D-Hierarchical SnS_2 Micro/Nano-structures: Controlled Synthesis, Formation Mechanism and Lithium Ion Storage Performances. *CrystEngComm* **2012**, *14*, 1364−1375.

(19) Zhai, C.; Du, N.; Zhang, H.; Yu, J.; Yang, D. Multiwalled Carbon Nanotubes Anchored with SnS_2 Nanosheets as High-Performance Anode Materials of Lithium-Ion Batteries. *ACS Appl. Mater. Interfaces* **2011**, *3*, 4067−4074.

(20) Zhang, Q.; Li, R.; Zhang, M.; Zhang, B.; Gou, X. SnS_2/Reduced Graphene Oxide Nanocomposites with Superior Lithium Storage Nerformance. *Electrochim. Acta* **2014**, *115*, 425−433.

(21) Zhang, L.; Zhao, K.; Xu, W.; Dong, Y.; Xia, R.; Liu, F.; He, L.; Wei, Q.; Yan, M.; Mai, L. Integrated SnO_2 Nanorod Array with Polypyrrole Coverage for High-rate and Long-life Lithium Batteries. *Phys. Chem. Chem. Phys.* **2015**, *17*, 7619−7623.

DOI: 10.1021/acsami.5b07044
ACS Appl. Mater. Interfaces 2015, 7, 23205−23215

(22) van Aken, P. A.; Liu, J.; Wen, Y.; Maier, J.; Yu, Y. In situ Reduction and Coating of SnS_2 Nanobelts for Fee-Standing SnS@Polypyrrole-Nanobelt/Carbon-Nanotube Paper Electrodes with Superior Li-Ion Storage. *J. Mater. Chem. A* **2015**, *3*, 5259−5265.
(23) Chang, K.; Chen, W.-x.; Li, H.; Li, H. Microwave-Assisted Synthesis of SnS_2/SnO_2 Composites by L-Cysteine and their Electrochemical Performances When Used as Anode Materials of Li-Ion Batteries. *Electrochim. Acta* **2011**, *56*, 2856−2861.
(24) Shi, W.; Lu, B. Nanoscale Kirkendall Effect Synthesis of Echinus-like SnO_2@SnS_2 Nanospheres as High Performance Anode Material for Lithium Ion Batteries. *Electrochim. Acta* **2014**, *133*, 247−253.
(25) Zhu, Q.; Wu, P.; Zhang, J.; Zhang, W.; Zhou, Y.; Tang, Y.; Lu, T. Cyanogel-Derived Formation of 3 D Nanoporous SnO_2−M_xO_y (M= Ni, Fe, Co) Hybrid Networks for High-Performance Lithium Storage. *ChemSusChem* **2015**, *8*, 131−137.
(26) Wu, Q.; Jiao, L.; Du, J.; Yang, J.; Guo, L.; Liu, Y.; Wang, Y.; Yuan, H. One-Pot Synthesis of Three-Dimensional SnS_2 Hierarchitectures as Anode Material for Lithium-Ion Batteries. *J. Power Sources* **2013**, *239*, 89−93.
(27) Wang, Q.; Nie, Y.-X.; He, B.; Xing, L.-L.; Xue, X.-Y. SnS_2−Graphene Nanocomposites as Anodes of Lithium-Ion Batteries. *Solid State Sci.* **2014**, *31*, 81−84.
(28) Chen, P.; Su, Y.; Liu, H.; Wang, Y. Interconnected Tin Disulfide Nanosheets Grown on Graphene for Li-Ion Storage and Photocatalytic Applications. *ACS Appl. Mater. Interfaces* **2013**, *5*, 12073−12082.
(29) Wu, P.; Wang, H.; Tang, Y.; Zhou, Y.; Lu, T. Three-Dimensional Interconnected Network of Graphene-Wrapped Porous Silicon Spheres: In Situ Magnesiothermic-Reduction Synthesis and Enhanced Lithium-Storage Capabilities. *ACS Appl. Mater. Interfaces* **2014**, *6*, 3546−3552.
(30) Liu, J.; Zhou, W.; Lai, L.; Yang, H.; Hua Lim, S.; Zhen, Y.; Yu, T.; Shen, Z.; Lin, J. Three Dimensionals α-Fe_2O_3/Polypyrrole (Ppy) Nanoarray as Anode for Micro Lithium Ion Batteries. *Nano Energy* **2013**, *2*, 726−732.
(31) Shen, L.; Che, Q.; Li, H.; Zhang, X. Mesoporous $NiCo_2O_4$ Nanowire Arrays Grown on Carbon Textiles as Binder-Free Flexible Electrodes for Energy Storage. *Adv. Funct. Mater.* **2014**, *24*, 2630−2637.
(32) Hu, L.; Ren, Y.; Yang, H.; Xu, Q. Fabrication of 3D Hierarchical MoS_2/Polyaniline and MoS_2/C Architectures for Lithium-Ion Battery Applications. *ACS Appl. Mater. Interfaces* **2014**, *6*, 14644−14652.
(33) Sun, Y.; Hu, X.; Luo, W.; Xia, F.; Huang, Y. Reconstruction of Conformal Nanoscale MnO on Graphene as a High-Capacity and Long-Life Anode Material for Lithium Ion Batteries. *Adv. Funct. Mater.* **2013**, *23*, 2436−2444.
(34) Balogun, M.-S.; Qiu, W.; Luo, Y.; Huang, Y.; Yang, H.; Li, M.; Yu, M.; Liang, C.; Fang, P.; Liu, P.; Tong, Y. Improving the Lithium-Storage Properties of Self-Grown Nickel Oxide: A Back-Up from TiO_2 Nanoparticles. *ChemElectroChem* **2015**, *2*, 1243−1248.
(35) Kang, J.-G.; Lee, G.-H.; Park, K.-S.; Kim, S.-O.; Lee, S.; Kim, D.-W.; Park, J.-G. Three-Dimensional Hierarchical Self-supported Multiwalled Carbon Nanotubes/Tin(iv) Disulfide Nanosheets Heterostructure Electrodes for High Power Li Ion Batteries. *J. Mater. Chem.* **2012**, *22*, 9330−9337.
(36) Jiang, X.; Yang, X.; Zhu, Y.; Shen, J.; Fan, K.; Li, C. In Situ Assembly of Graphene Sheets-Supported SnS_2 Nanoplates into 3D Macroporous Aerogels for High-Performance Lithium Ion Batteries. *J. Power Sources* **2013**, *237*, 178−186.
(37) Lu, X.; Yu, M.; Zhai, T.; Wang, G.; Xie, S.; Liu, T.; Liang, C.; Tong, Y.; Li, Y. High Energy Density Asymmetric Quasi-Solid-State Supercapacitor Based on Porous Vanadium Nitride Nanowire Anode. *Nano Lett.* **2013**, *13*, 2628−2633.
(38) Balogun, M.-S.; Yu, M.; Li, C.; Zhai, T.; Liu, Y.; Lu, X.; Tong, Y. Facile Synthesis of Titanium Nitride Nanowires on Carbon Fabric for Flexible and High-rate Lithium Ion Batteries. *J. Mater. Chem. A* **2014**, *2*, 10825−10829.
(39) Balogun, M.-S.; Qiu, W.; Wang, W.; Fang, P.; Lu, X.; Tong, Y. Recent Advances in Metal Nitrides as High-Performance Electrode Materials for Energy Storage Devices. *J. Mater. Chem. A* **2015**, *3*, 1364−1387.
(40) Chang, K.; Chen, W. L-cysteine-assisted Synthesis of Layered MoS_2/Graphene Composites with Excellent Electrochemical Performances for Lithium Ion Batteries. *ACS Nano* **2011**, *5*, 4720−4728.
(41) Huang, T.; Mao, S.; Zhou, G.; Wen, Z.; Huang, X.; Ci, S.; Chen, J. Hydrothermal Synthesis of Vanadium Nitride and Modulation of its Catalytic Performance for Oxygen Reduction Reaction. *Nanoscale* **2014**, *6*, 9608−9613.
(42) Xiong, Q.-q.; Tu, J.-p.; Xia, X.-h.; Zhao, X.-y.; Gu, C.-d.; Wang, X.-l. A Three-Dimensional Hierarchical Fe_2O_3@NiO Core/Shell Nanorod Array on Carbon Cloth: A New Class of Anode for High-Performance Lithium-Ion Batteries. *Nanoscale* **2013**, *5*, 7906−7912.
(43) Guan, C.; Wang, X.; Zhang, Q.; Fan, Z.; Zhang, H.; Fan, H. J. Highly Stable and Reversible Lithium Storage in SnO_2 Nanowires Surface Coated with a Uniform Hollow Shell by Atomic Layer Deposition. *Nano Lett.* **2014**, *14*, 4852−4858.
(44) Luo, Y.; Balogun, M.-S.; Qiu, W.; Zhao, R.; Liu, P.; Tong, Y. Sulfurization of FeOOH Nanorods on a Carbon Cloth and their Conversion into Fe_2O_3/Fe_3O_4-S Core-Shell Nanorods for Lithium Storage. *Chem. Commun.* **2015**, *51*, 13016−13019.
(45) Kim, T.-J.; Kim, C.; Son, D.; Choi, M.; Park, B. Novel SnS_2-Nanosheet Anodes for Lithium-Ion Batteries. *J. Power Sources* **2007**, *167*, 529−535.
(46) Cui, G.; Gu, L.; Thomas, A.; Fu, L.; van Aken, P. A.; Antonietti, M.; Maier, J. A Carbon/Titanium Vanadium Nitride Composite for Lithium Storage. *ChemPhysChem* **2010**, *11*, 3219−3223.
(47) Sun, Q.; Fu, Z.-W. Vanadium Nitride as a Novel Thin Film Anode Material for Rechargeable Lithium Batteries. *Electrochim. Acta* **2008**, *54*, 403−409.
(48) Zhang, K.; Wang, H.; He, X.; Liu, Z.; Wang, L.; Gu, L.; Xu, H.; Han, P.; Dong, S.; Zhang, C.; Yao, J.; Cui, G.; Chen, L. A Hybrid Material of Vanadium Nitride and Nitrogen-Doped Graphene for Lithium Storage. *J. Mater. Chem.* **2011**, *21*, 11916−11922.
(49) Wang, L.; Zhuo, L.; Yu, Y.; Zhao, F. High-Rate Performance of SnS_2 Nanoplates without Carbon-Coating as Anode Material for Lithium Ion Batteries. *Electrochim. Acta* **2013**, *112*, 439−447.
(50) Jiang, Z.; Wang, C.; Du, G.; Zhong, Y. J.; Jiang, J. Z. In Situ Synthesis of SnS_2@Graphene Nanocomposites for Rechargeable Lithium Batteries. *J. Mater. Chem.* **2012**, *22*, 9494−9496.
(51) Kim, H. S.; Chung, Y. H.; Kang, S. H.; Sung, Y.-E. Electrochemical Behavior of Carbon-Coated SnS_2 for Use as the Anode in Lithium-Ion Batteries. *Electrochim. Acta* **2009**, *54*, 3606−3610.
(52) Rahman, M.; Wang, J. Z.; Hassan, M. F.; Wexler, D.; Liu, H. K. Amorphous Carbon Coated High Grain Boundary Density Dual Phase $Li_4Ti_5O_{12}$-TiO_2: A Nanocomposite Anode Material for Li-Ion Batteries. *Adv. Energy Mater.* **2011**, *1*, 212−220.
(53) Wu, P.; Du, N.; Zhang, H.; Liu, J.; Chang, L.; Wang, L.; Yang, D.; Jiang, J.-Z. Layer-Stacked Tin Disulfide Nanorods in Silica Nanoreactors with Improved Lithium Storage Capabilities. *Nanoscale* **2012**, *4*, 4002−4006.
(54) Zhang, M.; Lei, D.; Yu, X.; Chen, L.; Li, Q.; Wang, Y.; Wang, T.; Cao, G. Graphene Oxide Oxidizes Stannous Ions to Synthesize Tin Sulfide−Graphene Nanocomposites with Small Crystal Size for High Performance Lithium Ion Batteries. *J. Mater. Chem.* **2012**, *22*, 23091−23097.
(55) Wang, Q.; Huang, Y.; Miao, J.; Zhao, Y.; Wang, Y. Synthesis and Electrochemical Characterizations of Ce doped SnS_2 Anode Materials for Rechargeable Lithium Ion Batteries. *Electrochim. Acta* **2013**, *93*, 120−130.
(56) Du, N.; Wu, X.; Zhai, C.; Zhang, H.; Yang, D. Large-Scale Synthesis and Application of SnS_2−Graphene Nanocomposites as Anode Materials for Lthium-Ion Batteries with Enhanced Cyclic Performance and Reversible Capacity. *J. Alloys Compd.* **2013**, *580*, 457−464.
(57) Zou, Y.; Wang, Y. Microwave Solvothermal Synthesis of Flower-like SnS_2 and SnO_2 Nanostructures as High-Rate Anodes for Lithium Ion Batteries. *Chem. Eng. J.* **2013**, *229*, 183−189.

DOI: 10.1021/acsami.5b07044
ACS Appl. Mater. Interfaces 2015, 7, 23205−23215

(58) Liu, S.; Yin, X.; Chen, L.; Li, Q.; Wang, T. Synthesis of Self-Assembled 3D Flowerlike SnS_2 Nanostructures with Enhanced Lithium Ion Storage Property. *Solid State Sci.* **2010**, *12*, 712−718.
(59) Xia, J.; Li, G.; Mao, Y.; Li, Y.; Shen, P.; Chen, L. Hydrothermal Growth of SnS_2 Hollow Spheres and their Electrochemical Properties. *CrystEngComm* **2012**, *14*, 4279−4283.
(60) Chang, B.-Y.; Park, S.-M. Electrochemical Impedance Spectroscopy. *Annu. Rev. Anal. Chem.* **2010**, *3*, 207−229.
(61) Balogun, M.-S.; Yu, M.; Huang, Y.; Li, C.; Fang, P.; Liu, Y.; Lu, X.; Tong, Y. Binder-free Fe_2N Nanoparticles on Carbon Txtile with High Power Density as Novel Anode for High-Performance Flexible Lithium Ion Batteries. *Nano Energy* **2015**, *11*, 348−355.
(62) Macdonald, D. D. Reflections on the History of Electrochemical Impedance Spectroscopy. *Electrochim. Acta* **2006**, *51*, 1376−1388.
(63) Shu, D.; Cheng, H.; Lv, C.; Asi, M. A.; Long, L.; He, C.; Zou, X.; Kang, Z. Soft-Template Synthesis of Vanadium Oxynitride-Carbon Nanomaterials for Supercapacitors. *Int. J. Hydrogen Energy* **2014**, *39*, 16139−16150.
(64) Choi, D.; Blomgren, G. E.; Kumta, P. N. Fast and Reversible Surface Redox Reaction in Nanocrystalline Vanadium Nitride Supercapacitors. *Adv. Mater.* **2006**, *18*, 1178−1182.
(65) Glaser, A.; Surnev, S.; Netzer, F.; Fateh, N.; Fontalvo, G.; Mitterer, C. Oxidation of Vanadium Nitride and Titanium Nitride Coatings. *Surf. Sci.* **2007**, *601*, 1153−1159.
(66) Merdrignac-Conanec, O.; El Badraoui, K.; L'Haridon, P. Nitridation under Ammonia of High Surface Area Vanadium Aerogels. *J. Solid State Chem.* **2005**, *178*, 218−223.
(67) Zhai, T.; Lu, X.; Ling, Y.; Yu, M.; Wang, G.; Liu, T.; Liang, C.; Tong, Y.; Li, Y. A New Benchmark Capacitance for Supercapacitor Anodes by Mixed-Valence Sulfur-Doped V_6O_{13-x}. *Adv. Mater.* **2014**, *26*, 5869−5875.
(68) Yu, M.; Zeng, Y.; Han, Y.; Cheng, X.; Zhao, W.; Liang, C.; Tong, Y.; Tang, H.; Lu, X. Valence-Optimized Vanadium Oxide Supercapacitor Electrodes Exhibit Ultrahigh Capacitance and Super-Long Cyclic Durability of 100 000 Cycles. *Adv. Funct. Mater.* **2015**, *25*, 3534−3540.
(69) Chao, D.; Xia, X.; Liu, J.; Fan, Z.; Ng, C. F.; Lin, J.; Zhang, H.; Shen, Z. X.; Fan, H. J. A V_2O_5/Conductive-Polymer Core/Shell Nanobelt Array on Three-Dimensional Graphite Foam: A High-Rate, Ultrastable, and Freestanding Cathode for Lithium-Ion Batteries. *Adv. Mater.* **2014**, *26*, 5794−5800.
(70) Wang, Q.; Sun, J.; Wang, Q.; Zhang, D.-a.; Xing, L.; Xue, X. Electrochemical Performance of α-MoO_3−In_2O_3 Core−Shell Nanorods as Anode Materials for Lithium-Ion Batteries. *J. Mater. Chem. A* **2015**, *3*, 5083−5091.
(71) Wang, Q.; Zhang, D.-A.; Wang, Q.; Sun, J.; Xing, L.-L.; Xue, X.-Y. High Electrochemical Performances of α-MoO_3@ MnO_2 Core-Shell Nanorods as Lithium-Ion Battery Anodes. *Electrochim. Acta* **2014**, *146*, 411−418.
(72) Luo, Y.; Luo, J.; Jiang, J.; Zhou, W.; Yang, H.; Qi, X.; Zhang, H.; Fan, H. J.; Yu, D. Y. W.; Li, C. M.; Yu, T. Seed-assisted Synthesis of Highly Odered TiO_2@α-Fe_2O_3 Core/Shell Arrays on Carbon Textiles for Lithium-Ion Battery Applications. *Energy Environ. Sci.* **2012**, *5*, 6559−6566.

DOI: 10.1021/acsami.5b07044
ACS Appl. Mater. Interfaces 2015, 7, 23205−23215